Chapter 3
Conformational and structural stability of propylthiol

3.1 Introduction

n-Propanethiol (nP) and 2-propanethiol (2P) are molecules of importance in astrochemistry [118] . Precise knowledge of the lowest energy conformers is of paramount significance. nP can take up seven possible conformers, namely trans–trans (T–T), trans–gauche (T–G), gauche–trans (G–T), gauche–gauche (G–G), gauche–gauche (G–G′), trans–gauche (T–G′), and gauche–trans (G′–T) and 2P has two conformers namely, anti (T) and gauche (G). as given in Fig. 3.1. In experiments, not all these conformers are found, though. Different researchers reported varying numbers and structures of conformers using different spectroscopic techniques like microwave [119-122], infrared [123, 124], Raman [125], and vacuum ultraviolet mass-analysed threshold ionization spectroscopy [87]. On the other hand, literature pertaining to computational research using methods such as Urey–Bradley force field theory [126], quantum molecular force field theory [92], MP2/cc-pVTZ, and B3LYP/6-311++G(2df, 2pd) [87] differed significantly among each other as well as from the experiments.

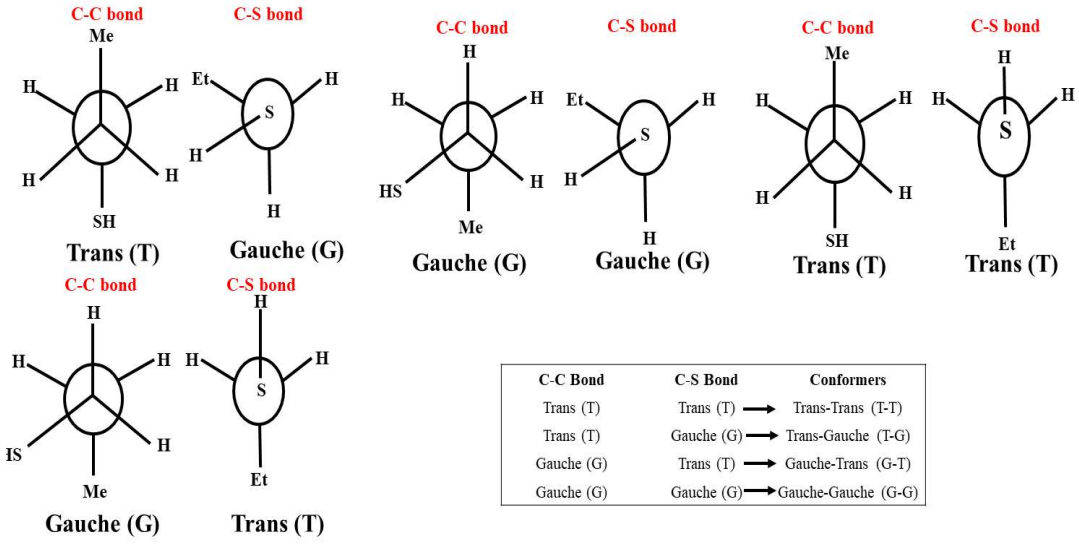

Figure 3.1 Newman projection for conformers of nP molecule with respect to C-C and C-S bonds.

Whereas the infrared absorption-based experiments detected the conformers T–T and G–T [123] as the global and local minima, respectively, the microwave-based rotational spectroscopic studies [120] reported that T–G and T–T were the global and local minimum, respectively. The matrix-assisted threshold ionization spectroscopy reported by Choi et al. observed only two conformers, T–G and G–G [87]. Based on their computational predictions using Franck–Condon calculations, they identified T–G as the global minimum and G–G as the other low-lying conformer amongst the five conformers (T–G < G–G < G–G′ < T–T < G–T) using B3LYP/6-311++G(2df, 2pd) level of theory [87]. The most recent work in this regard was done by Gorai et al., who predicted similar order of the conformers' energy as T–G < G–G < G–G′ < T–T < G–T using B3LYP/6-311++G(2df, 2pd) level of theory. Although Choi et al. [87] and Gorai et al. [118] employed an identical level of theory, their computational results varied significantly albeit the global minimum identified by both was T–G, as mentioned above.

It is noteworthy to say that the predictions shown in this report match extremely well with those of experimental predictions [120,123]. Despite Choi et al.'s disparity in identifying the correct local minima conformers, they ascribe the erroneous conformer to the experimentally observed one based on Franck–Condon calculations. The most recent predictions by Gorai et al. are also farther from experimental results.

Although Hayashi et al. reported T–G as the global minimum conformer of nP by carrying out the rotationally resolved spectroscopy [120] and subsequent works based on other experiments relied on the computational predictions in ascribing the correct conformational

information to the structures detected in their experiments, furthermore, in the case of 2P, the value corresponding to the rotational barrier needs revision as the latest theoretical work [92] cites a relatively older experimental observation [83] completely ignoring the latest experimental value [127] for no understandable reasons. Hence the accuracy and correctness of the computational prediction are of paramount importance as they go beyond merely supporting the experimental findings. Furthermore, there is no consensus on the correct sequence of the energies and the number of other low-energy conformers. In other words, the rationale for using the computational predictions to support the experimental findings is not completely satisfactory.

In order to fill the gaps pertaining to the low energy conformations of nP and 2P molecules, we re-investigated the conformational and structural stability of the propylthiol molecule using state of the art computational methods. The results reported herein correlate exceedingly well with the available experimental results for the propylthiol molecular system [87,118–120,123,124,126]. Computations of normal modes and electrostatic potential charge (ESP), Mullikan charge analysis (MCA), natural bond orbital analysis (NBO), frontier molecular orbital (FMO), and non-covalent interaction (NCI) were also carried out to support further the results pertaining to the conformational stability of nP and 2P molecules. It is envisaged that with the results reported herein, the unambiguity pertaining to the conformational aspects of nP would cease, and these results may serve as a benchmark for conformational analysis of the propylthiol molecular system.

3.2 Computational methods

Geometry optimizations, normal mode calculations, and natural bond orbital analysis (NBO) for all conformers of nP and 2P were carried out using the CCSD/cc-pVDZ level of theory. Potential energy surface was also generated at the CCSD/cc-pVDZ level of theory with step size 5° (containing 73 points) and variation in all the dihedral angles such as 1–5–8–11, 5–8–11–12, 6–5–8–11, and 6–5–8–9 [atom numbering as per Fig. 3.2]. A potential energy surface was also generated at the B3LYP/6-311++G(2df, 2pd) level of theory by varying the dihedral angles 1–5–8–11, and 5–8–11–12 with a step size of 10° and 5° (refer Fig. 2.5). A 2-dimensional potential energy surface was generated by simultaneously varying two dihedral angles, namely 1–5–8–11 and 5–8–11–12 with a step size of 30° (containing 144 points) at CCSD/cc-pVDZ level of theory [atom numbering as per Fig. 3.2]. Single point calculations were performed at HF, MP2, MP3, MP4, CCSD, and CCSD(T) levels of theory using cc-pVNZ (where N= D, T, Q) basis sets for all conformers of nP. Helgaker method was utilized to extrapolate correlation energy, and results were obtained with basis sets cc-pVNZ (where N = T, Q) [67]. Corresponding to low energy conformers, Mullikan charge analysis (MCA), electrostatic potential charge (ESP), non-covalent interaction (NCI) representation, natural bond orbital (NBO) analysis, and frontier molecular orbital (FMO) analysis were performed at the CCSD/cc-pVDZ level of theory. For population analysis done by using the Boltzmann distribution equation [128]. MultiWFN software was used for NCI calculations [69], and Gaussian 16 [68] was utilized for all other calculations.

3.3 Result and discussion

Optimized geometries of the low energy conformers of nP and 2P molecules are shown in Fig. 3.2 and 3.3 All these geometries were bereft of any imaginary frequency (Table 3.1 summarizes normal mode analysis).

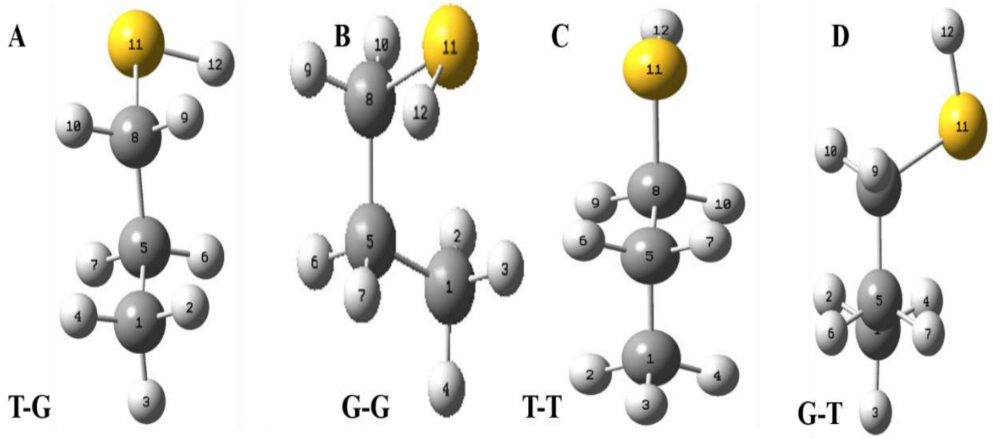

Figure 3.2 Optimized geometries of different conformers of nP at CCSD/cc-pVDZ level of theory. (configuration of conformers T-T, G-T, and T-G are given correspond C-C and C-S bonds respectively and here T represents Trans and G represents Gauche conformation and atoms are numbered for describing their properties elsewhere in the text)

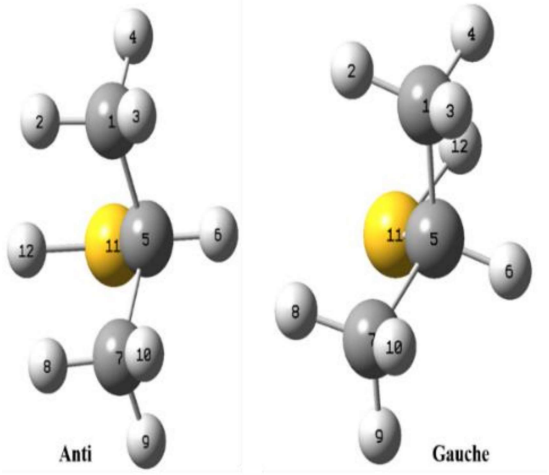

Figure 3.3 Optimized geometries of conformers of 2P molecule at CCSD/cc-pVDZ level of theory (Atoms are numbered for describing their properties elsewhere in the text)

The geometric parameters, whose experimental values are available, are summarized in Table 3.2 for nP and 2P molecules, and the same computed at CCSD/cc-pVDZ support the experimental results very well, which have hitherto not been reported in the computational literature. Taking a cue from this, the CCSD/cc-pVDZ has been used further for the remaining calculations for both nP and 2P molecules.

Table 3.1 Fundamental vibrational [Infrared (IR)] frequencies (cm^{-1}) of the conformers of nP and 2P molecules at CCSD/cc-pVDZ level of theory

n-propanethiol (nP)			
T-T	T-G	Experimental [118–120]	Tentative assignment
183	211	178	τ_{S-H}
357	367	329	δ_{C-C-C}
753	715	700	ν_{C-S}
756	748	728	ρ_{CH2}
875	815	814	δ_{S-H}
1147	1143	1105	ν_{C-C}
1252	1258	1243	τ_{CH2}
1275	1280	1300	ω_{CH2}
1390	1384	1351	ω_{CH2}
1423	1421	1384	δ_{CH3}
1491	1477	1456	ρ_{CH2}
2731	2725	2598	ν_{S-H}
3055	3054	2838	$\nu_{CH3(s)}$
3063	3062	2848	$\nu_{CH2(s)}$
3076	3077	2945	$\nu_{CH2(s)}$
3102	3105	2960	$\nu_{CH2(a)}$

3130	3129	3090	ν CH2(a)
3142	3142	3183	ν CH3(a)
2-propanethiol (2P)			
Anti	Gauche	Experimental [118–120]	
211	197	185	τ S-H
250	253	245	τ_{CH3}
277	273	310	τ_{CH3}
332	306	325	δ C-C-S
409	414	410	δ C-C-C
635	652	620	ν C-S
873	875	853	δ S-H
934	938	955	ρ CH3
967	1085	1063	ρ CH3
1118	1172	1082	ν C-C
1312	1364	1314	ω_{CH3}
1348	1413	1389	ω_{CH3}
1410	1423	1448	ω_{CH3}
2716	2727	2572	ν S-H
3050	3051	2927	ν CH3(s)

Fig. 3.4 also shows the potential energy curve generated through a relaxed scan on rotating the C–C and C–S bonds of the nP molecule where the dihedral angle was varied in steps of 5°, and the optimized geometry of the T–T and G–G conformers were the starting geometry. Four such potential energy curves were obtained corresponding to dihedral angles 1, 5, 8, 11 (C–C–C–S); 5, 8, 11, 12 (C–C–S–H); 6, 5, 8, 11 (H–C–C–S), and 6, 5, 8, 9 (H–C–C–H). These

scanning coordinates resulted in two conformers with minimum energy, as shown in Fig. 3.4 and 3.5 and Table 3.2.

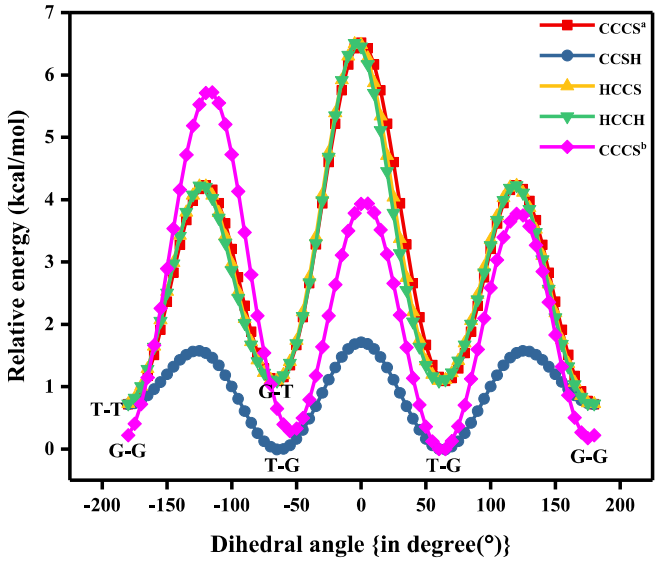

Figure 3.4 Various relative potential energy curves obtained at CCSD/cc-pVDZ level of theory with respect to T-G conformer. (clockwise relaxed scan with step size 5º) for nP molecule. (in image term 'a' and 'b' represent optimized geometry of T-T and G-G conformer that was taken into consideration)

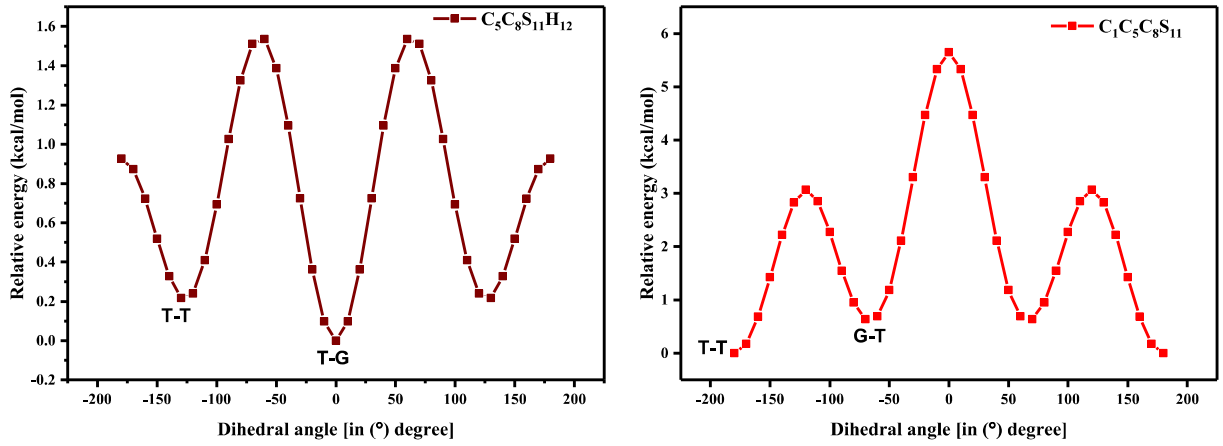

Figure 3.5 Potential energy surface plots generated for nP molecule correspond to (A) C-S and (B) C-C bonds with step size 10º at B3LYP/6-311++G (2df 2pd) level of theory.

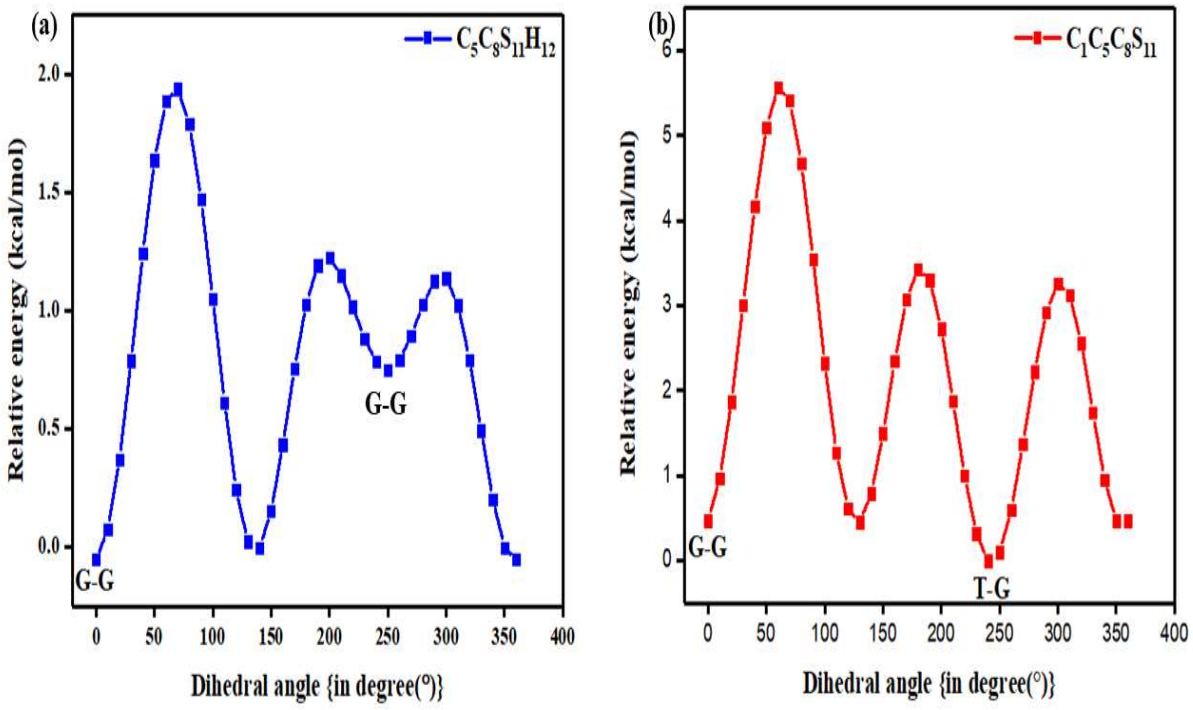

Figure 3.6 Potential energy surface plots generated for nP molecule correspond to (a) C-S and (b) C-C bonds with step size 10º at CCSD/cc-pVDZ level of theory.

Scanning coordinates 1, 5, 8, 11; 6, 5, 8, 11 and 6, 5, 8, 9 provide T–T and G–T conformers as a minimum, whereas T–G and T–T conformers were found corresponding to the dihedral angle 5, 8, 11, 12, which is similar to the one reported by Hayashi et al. [123] and Nakagawa et al. [120] respectively. Experimental measurements reported T–G as the global minimum (although one earlier experiment based on IR absorption identified T–T as the global minimum) with one local minimum conformer G–T or T–T conformers, respectively [119–125].

Table 3.2. Geometrical parameters and rotational barriers of the different conformers of the nP & 2P molecules at CCSD/cc-pVDZ level of theory [symbols R, A, and D represents the bond distance (angstrom (Å)), bond angle (º), and dihedral angle (º) respectively]

Geometrical parameters (n-propanethiol)						
Parameter[$]	T-T	Exp. [120]	T-G	Exp.[120]	G-G	G-T
R(1,2)	1.11	1.1	1.11	1.09	1.11	1.11
R(1, 5)	1.53	1.54	1.54	1.54	1.53	1.54
R(8, 11)	1.84	1.81	1.84	1.82	1.84	1.85
R(11, 12)	1.35	1.34	1.35	1.34	1.35	1.3
A(2, 1, 5)	111º 30′	111º 0′	111º 48′	111º 0′	110º 41′	110º.45′
A(5, 8, 11)	109º 33′	108º 34′	114º 10′	113º 37′	114º 52′	110º 24′
A(8, 11, 12)	96º 27′	96º 13′	96º 10	96º 00′	95º 53′	96º 36′
D(5,8,11,12)	-180º 00′	180º 00′	-63º 17′	61º 45′	-65º 15′	-176º 38′

Geometrical parameters (2-propanethiol)				Rotational energy Barrier (C-S) at CCSD/cc-pVDZ level of theory			
Parameter[$]	Gauche	Anti	Experimental[$$]	Our results		Experiment [120,127] (kcal/mol)	
R (1, 2)	1.11	1.11	1.09[a]				
				nP	2P	nP	2P
R (1, 5)	1.53	1.53	1.52[a]				
R (5, 11)	1.85	1.85	1.85[a]				
R (11, 12)	1.35	1.35	1.35[a]				
A (4, 1, 5)	111º 30′	111º 12′	113º 36′ [a]	1.58 1.54[b]	1.72	1.31	1.88
A (1, 5, 11)	111º 48′	111º 48′	111º 12′ [a]				
A (5, 11, 12)	96º 12′	95º 36′	96º 30′ [a]				

[$]Atom numbering patterns are as per Fig. 3.2 and 3.5
[$$] 'a' :geometrical parameters of 'anti' corresponding to C–S; 'b': rotational barrier at B3LYP/6-311++G (2df, 2pd) level of theory

The scan with initial geometry as the optimized G–G conformer resulted in T–G as the global minimum conformer and G–G as the local minimum which is similar to the prediction by Gorai et al. [118] and Choi et al. [87]. Furthermore, the results reported herein match exceedingly well with the experimental results. Table 3.3 summarizes all conformational scans for the nP molecule at the CCSD/cc-pVDZ level of theory with a step size of 5°.

Table 3.3 Summary of conformational analysis of nP molecule via relaxed scan at CCSD/cc-pVDZ level of theory.

Scan coordinate[$]	Global minimum	Local minimum	Rotational barrier (kcal/mol)	ΔE (kcal/mol)[$$]	Experiment (kcal/mol)
$C_1C_5C_8S_{11}$	T-T	G-T	3.14 (C-C)	0.37	
$C_5C_8S_{11}H^a_{12}$	T-G	T-T	1.58 (C-S)	0.72	1.31[118]
$H_6C_5C_8H_9$	T-T	G-T	3.13 (C-C)	0.36	
$H_6C_5C_8S_{11}$	T-T	G-T	3.10 (C-C)	0.38	
$C_1C_5C_8S_{11}$	T-G	G-G	3.93 (C-C)	0.22	
$C_5C_8S_{11}H^b_{12}$	G-G	G-G’	2.24 (C-S)	0.12	1.31[118]

$: Atom labels as per the Fig. 3.2
a: optimized geometry of T-T conformer; b: optimized geometry of G-G conformer, have been taken into consideration
$$: ΔE = Local minimum - Global minimum

The C–S rotational barrier of the nP molecule is computed to be 1.58 kcal/mol and 2.24 kcal/mol from the corresponding scans with initial geometries T–T and G–G, respectively where the experimental value for the C–S rotational barrier is 1.31 kcal/mol.

It was observed that when the scan was carried out by varying the CCSH dihedral angle, the C–C bond got significantly distorted (up to 13%), and the C–S bond got distorted up to

5.4%. It is evident that the C–C bond plays a crucial role in determining the low energy conformer along with the C–S bond. This reinforces the fact that along with the C–S bond, the C–C bond should be considered to render the conformational analysis of the nP molecule complete. Past research reports have only resorted to the C–S bond rotation.

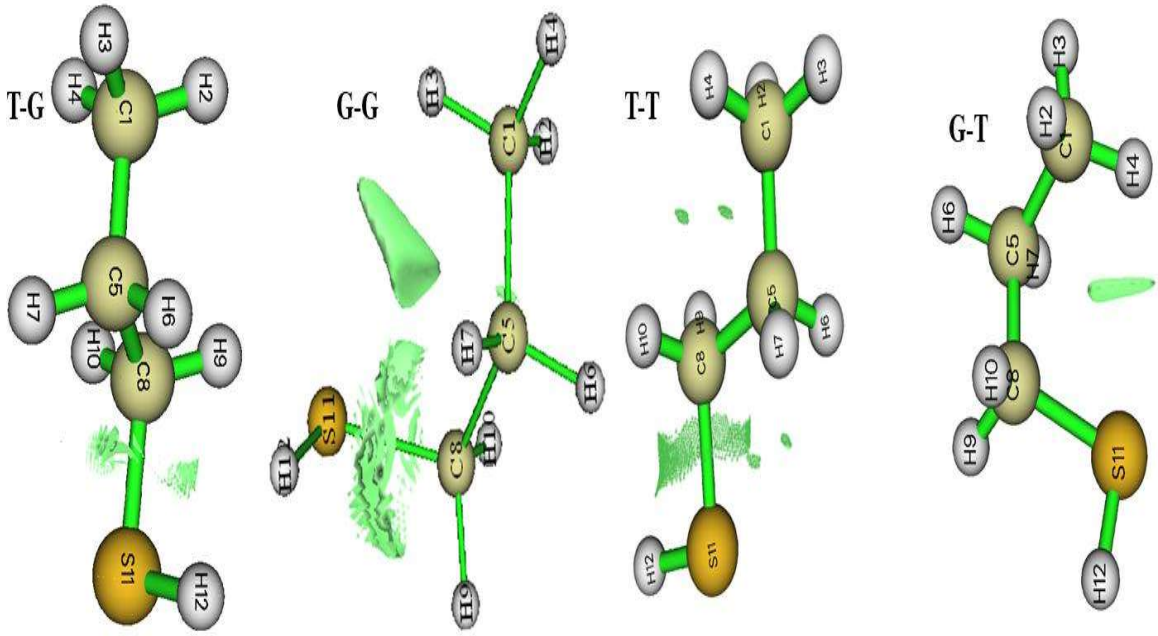

Figure 3.7 NCI Plot of conformers T-G, G-G, T-T, and G-T of nP molecule at CCSD/cc-pVDZ level of theory.

Although both C–C and C–S bonds were considered for the analysis reported herein, the analysis was carried out separately. Taking a cue from the individual analysis *i.e.*, the rotations distort the bonds, calculations were extended further (Fig. 3.8) where both the rotations were carried out simultaneously. The resulting potential energy 2D surface revealed T–T as the global minimum instead of the T–G conformer when we considered T–T optimized geometry as the starting conformation. With the optimized geometry of the G–G conformer as the initial

point for the double scan varying the C–S and C–C bond simultaneously is shown in Fig. 3.9. The global minimum conformer obtained from the 2D scan of the T–T conformer and the global minimum got from the three C–C bond rotations (Fig. 3.4) were identical.

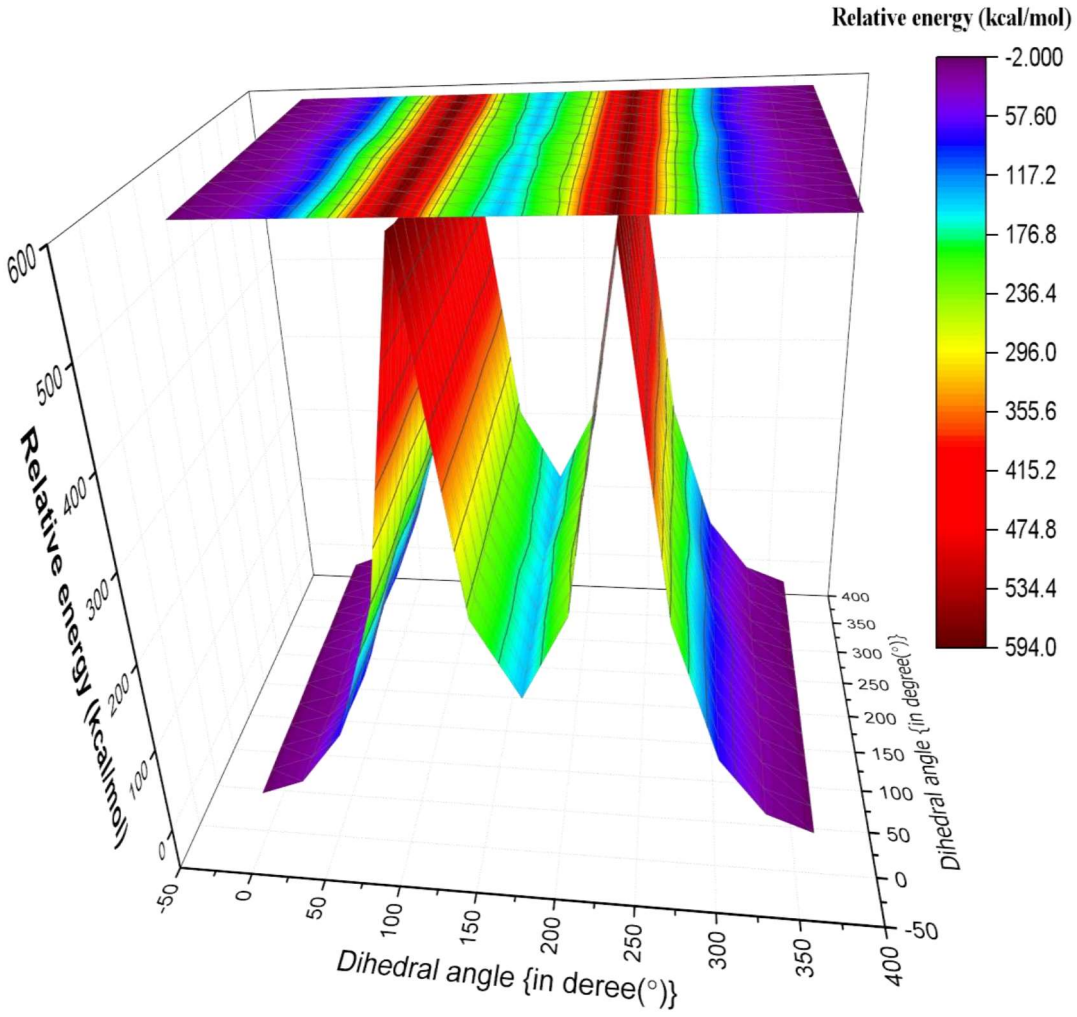

Figure 3.8 Potential energy surface plot generated for nP molecule with two coordinates (CCCS and CCSH) with step size 30º at CCSD/cc-pVDZ level of theory. (geometry of T-T conformer as a starting molecule)

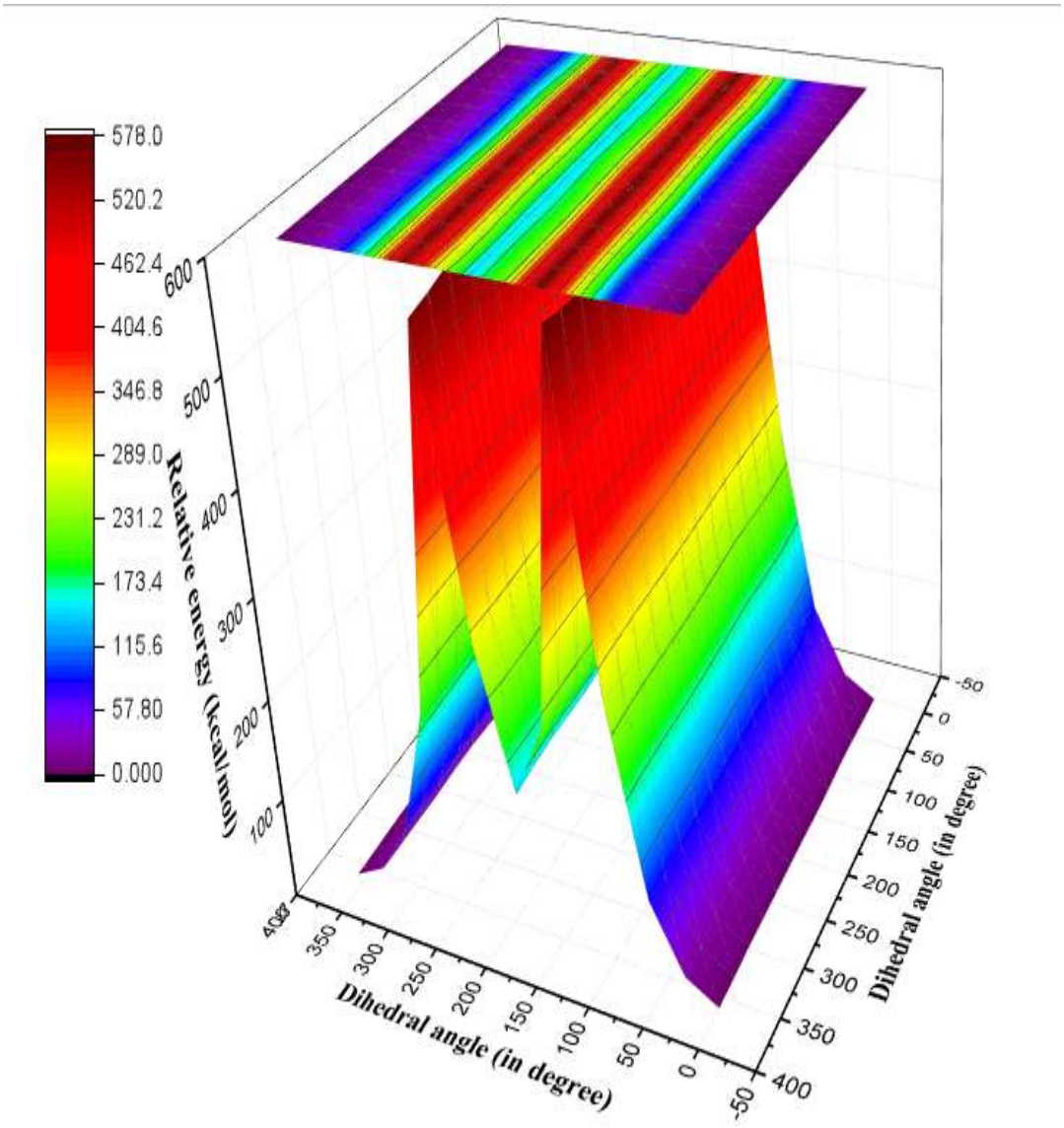

Figure 3.9 Potential energy surface plot generated for nP molecule with two coordinates (CCCS and CCSH) with step size 30º at CCSD/cc-pVDZ level of theory. (geometry of G-G conformer as a starting molecule)

The computed value of the rotational barrier (Table 3.3) for the nP molecule corresponding to the three C–C bond rotations is 3.1 ± 0.2 kcal/mol which too matches well with the experimental value of 2.9 kcal/mol [129].

In Fig. 3.4 the T–G conformer is taken as the reference and the energies of other conformers are depicted with respect to this reference. In the studied models, the total energy of the nP molecule was calculated concerning dihedral angle, which is summarized in Tables 3.5 and 3.4.

Table 3.4 Relative change in energy (kcal/mol) of the local minima conformers of the nP and 2P molecules with respect to the global minimum conformer at different levels of theory.

Basis set→	cc-pVDZ		cc-pVTZ		cc-pVQZ		CBS limit		Experiment	
Methods↓	nP	2P	nP	2P	nP	2P	nP	2P	nP	2P
HF	0.48	0.14	0.68	0.04	0.75	0.06	0.78	0.070	0.38	0.06
MP2	0.01	0.35	0.11	0.10	0.13	0.04	0.16	0.004		
MP3	0.18	0.36	0.25	0.10	0.28	0.06	0.30	0.031		
MP4	0.17	0.36	0.22	0.10	0.26	0.06	0.28	0.031		
CCSD	0.19	0.32	0.25	0.12	0.28	0.03	0.30	0.032		
CCSD(T)	0.14	0.37	0.17	0.11	0.20	0.06	0.22	0.030		

Table 3.5 Relative change in single-point energy (kcal/mol) of the local minima conformer of the nP (T-T) and 2P with respect to the global minimum conformer (T-G for nP) at different levels of theory.

Basis set→	CBS limit		Experiment		Optimized energy by Choi et al @B3LYP/6-311++G(2df 2pd) [87]	
Methods↓	nP	2P	nP [120]	2P [127]	nP	2P
HF	0.78	0.07	0.38	0.06	0.62 (TG-TT) 0.50 (TG-GG)	0.05
MP2	0.16	0.00				
MP3	0.30	0.03				
MP4	0.28	0.03				
CCSD	0.30	0.03				
CCSD(T)	0.22	0.03				

The energy difference between the global minimum (T–G) and the local minima (G–G), calculated at the CCSD(T)/CBS limit, was 0.30 kcal/mol, which matched very well with the experimental value (0.38 kcal/mol) as shown in Tables 3.5 and 3.4 [120]. However, the value of the energy difference turned out to be 0.22 kcal/mol when the geometries were optimized at the CCSD/cc-pVDZ level of theory. Apart from this, the relative energy of the other two conformers is 0.71 kcal/mol and 1.08 kcal/mol for T–T and G–T conformers at the CCSD/cc-pVDZ level of theory, respectively. The predicted energy difference was further verified by carrying out population analysis, summarized in Table 3.6. From Table 3.6, it is evident that when the entire conformational space is explored by varying the C_α–S and the C_α–C_β bonds, the conformers T–G and G–G seem to have the maximum populations followed by the T–T conformer. Earlier computational works concentrated only on the C_α–S, which was adequate to understand the global minimum but predictions varied for the local minimum. Herein it is shown unambiguously that the C_α–C_β should also be considered for the accurate prediction of the local minima conformer. Our results support all previous experimental measurements [119–124].

Table 3.6 Conformational abundance of nP and 2P molecules at CCSD/cc-pVDZ level of theory. (ΔE in kcal/mol and N_f expressed in %)

Dihedral angle	nP										2P	
	1,5,8,11[a] (CCCS)		5,8,11,12[a] (CCSH)		6,5,8,11[a] (HCCS)		6,5,8,9[a] (HCCH)		1,5,8,11[b] (CCCS)		6,5,11,12 HCSH	
	ΔE	N_f	ΔE	N_f	ΔE	N_f	ΔE	N_f	ΔE	N_f	ΔE	N_f
0°	0.0	33.8	0.7	10.7	0.0	33.4	0.0	33.2	0.2	23.0	0.0	30.1
60°	3.5	0.1	1.5	2.7	3.5	0.1	3.5	0.1	5.7	0.0	1.7	1.6
120°	0.4	16.1	0.0	35.7	0.5	15.3	0.5	15.5	0.3	20.4	0.3	17.5
180°	5.8	0.0	1.7	2.0	5.8	0	5.7	0.0	4.0	0.0	1.8	1.5
240°	0.4	16.1	0.0	35.7	0.4	17.8	0.4	17.9	0.0	33.3	0.3	17.5
300°	3.5	0.1	1.5	2.7	3.5	0.1	3.5	0.1	3.9	0.0	1.7	1.6
360°	0.0	33.8	0.7	10.7	0.0	33.4	0.0	33.2	0.2	23.0	0.0	30.1

Note:
1.Population of different conformers was calculated using the Boltzmann distribution equation, $N = \frac{e^{-\Delta E/RT}}{\sum_n e^{-\Delta E_n/RT}}$; where ΔE represents the difference in energy of conformer with respect to the global minima conformer and summation applied over all n possible conformers, $R = 1.987 \times 10^{-3}$ kcal/K *mol and $T = 298$ K).
2. Here terms 'a' and 'b' represents T-T and G-G conformation of the initial geometry that was used for the conformational analysis respectively.

In the case of the 2-propanethiol (2P) molecule, a homologue of the nP molecule, no change in conformation was observed even after revisiting the calculations with higher levels of theory compared to the ones reported earlier. Similar to earlier reports [83,127], only two low-energy conformers were observed, with the anti-conformer being the global minimum and the gauche conformer being the local minimum, as shown in Fig. 3.10 and 3.3.

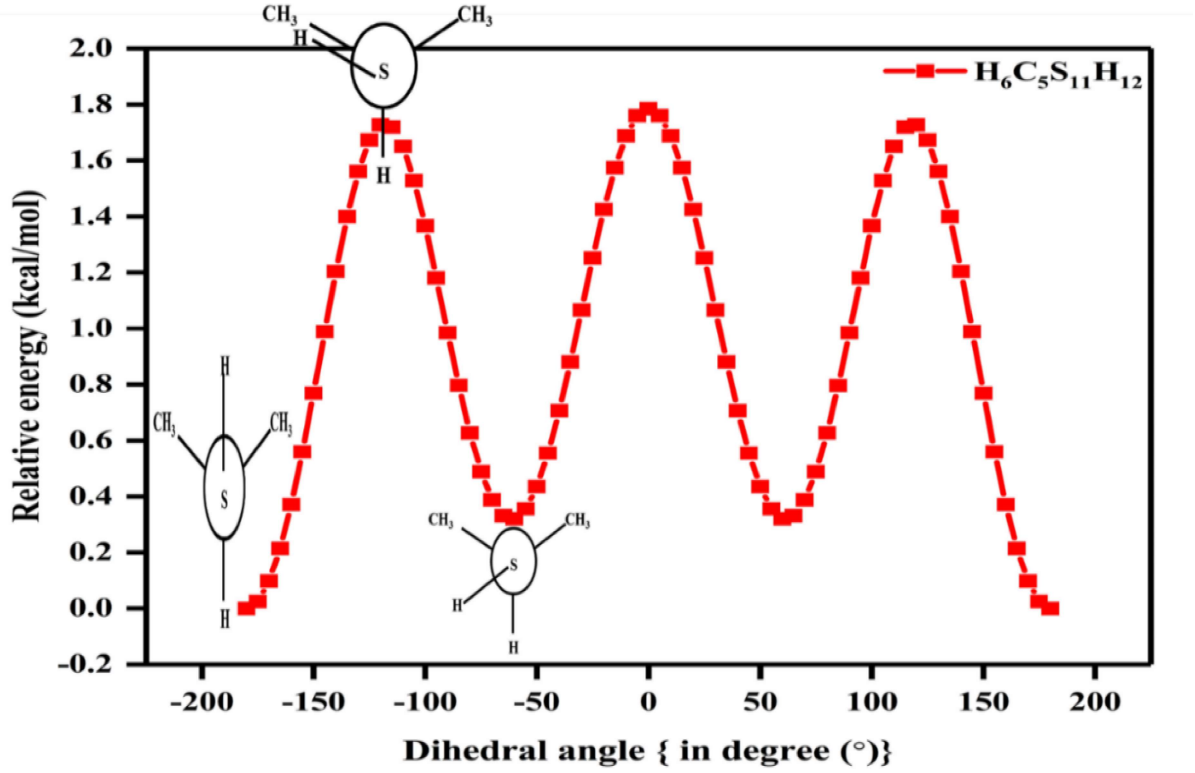

Figure 3.10 Potential energy surface plot of 2P molecule at CCSD/cc-pVDZ level of theory with respect to C-S bond. (clockwise relaxed scan of step size 5º)

The potential energy surface corresponding to the HCSH dihedral angle with a step size of 5° from 0 to 360° was generated. The rotational barrier corresponding to the C–S bond was 1.72 kcal/mol, closer to the experimentally measured value of 1.88 kcal/mol [127]. The energy difference between these conformers was calculated (single-point energy) to be 0.03 kcal/mol at the CCSD(T)/CBS limit as given in Tables 3.5 and 3.8, where the experimentally measured value was 0.06 kcal/mol. The population analysis summarized in Table 3.6 reinforces anti conformer being the global minimum and gauche as the local minimum. The stability of conformers of 2P molecules was well correlated with the NCI plots, as shown in Fig. 3.11.

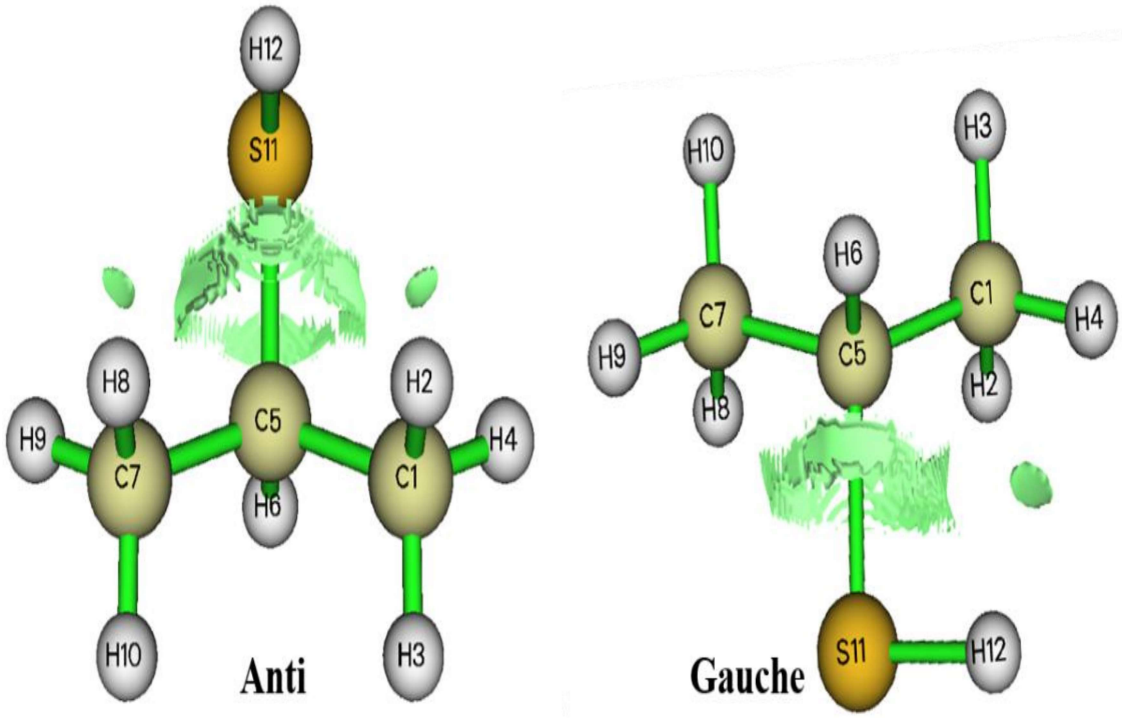

Figure 3.11 NCI Plot of conformers anti, and gauche of 2P molecule at CCSD/cc-pVDZ level of theory.

The thermodynamic parameters of conformers T–G and G–G of nP molecule and for conformers anti and gauche of 2P molecule are summarized in Table 3.7. Fausto et al. [92] predicted 3.7 kcal/mol and cited Don Smith et al.'s experimental work of 1968 based on infrared absorption spectroscopy for the rotational barrier of 2P [83]. However, Griffith et al. carried out microwave absorption spectroscopy in 1975, adding accuracy to the earlier observed conformers of 2P [127]. Griffith et al. reported 1.88 kcal/mol as the rotational barrier, and it is beyond our comprehension as to why Fausto et al. cited Don Smith's work but ignored Griffith's. It must be noted that the values for the rational barrier predicted and reported in this work match exceedingly well with the values observed by Griffith et al.

Table 3.7 Thermodynamic parameters of conformers of nP and 2P molecules at CCSD/cc-pVDZ level of theory (all parameters are in kJ/mol)

Thermodynamic Parameters	nP			2P	
	T-G	G-G	T-T	Anti	Gauche
Gibbs Free energy (x10^6)	-1.36	-1.36	-1.36	-1.36	-1.36
Enthalpy (x10^6)	-1.36	-1.36	-1.36	-1.36	-1.36
Entropy	0.32	0.31	0.32	0.31	0.31
Heat capacity	0.08	0.08	0.08	0.09	0.09

Thermodynamic parameters also help in the elucidation of the stability of molecules [130]. So for this, we computed thermodynamic parameters at our benchmark functional CCSD/cc-pVDZ because results of this functional matched exceedingly well with experimental results, which is summarized in Table 3.10. From Table 3.10, it is evident that the conformer T-G is the global minimum for nP molecule and anti is the global minimum for 2P molecule. Thermodynamic results reinforced the predictions of FMO analysis where conformer T-G is the thermodynamically favorable conformer of nP molecule and anti-conformer is the kinetically and thermodynamically favorable conformer for 2P molecule.

3.3.1 Electrostatics potential (ESP) surface plot

Electrostatic potential (ESP) surface analysis helps to understand the molecule's chemical reactivity [131]. The computed ESP map of nP is shown in Fig. 3.12, and the corresponding charges are depicted in Table 3.8. From Table 3.8, it is clear that the sulfur atom (S_{11}) behaves as an electrophilic center in all conformers. Specifically, the conformer T–T shows the highest values compared to T–G, G–G, and G–T. The electrophilicity of the C_1 atom was seen to be

the maximum in the T–T conformer and the third highest in the T–G conformer, whereas conformer G–G shows the least electrophilicity. The variation in the electrophilicity is the direct consequence of the variation in the extent to which the C_1 atom interacts with the sulfur atom's lone pair of electrons. The major nucleophilic center is the C_5 atom in T–T, T–G, and G–G conformers of the nP molecule. In the G–G conformer, the H_{10} atom strongly interacts with the lone pair of the sulfur atom, but atom H_9 shows weak interaction compared to T–T conformers. ESP charge also confirms that the conformer G–G and T–G are the thermodynamically favorable conformers

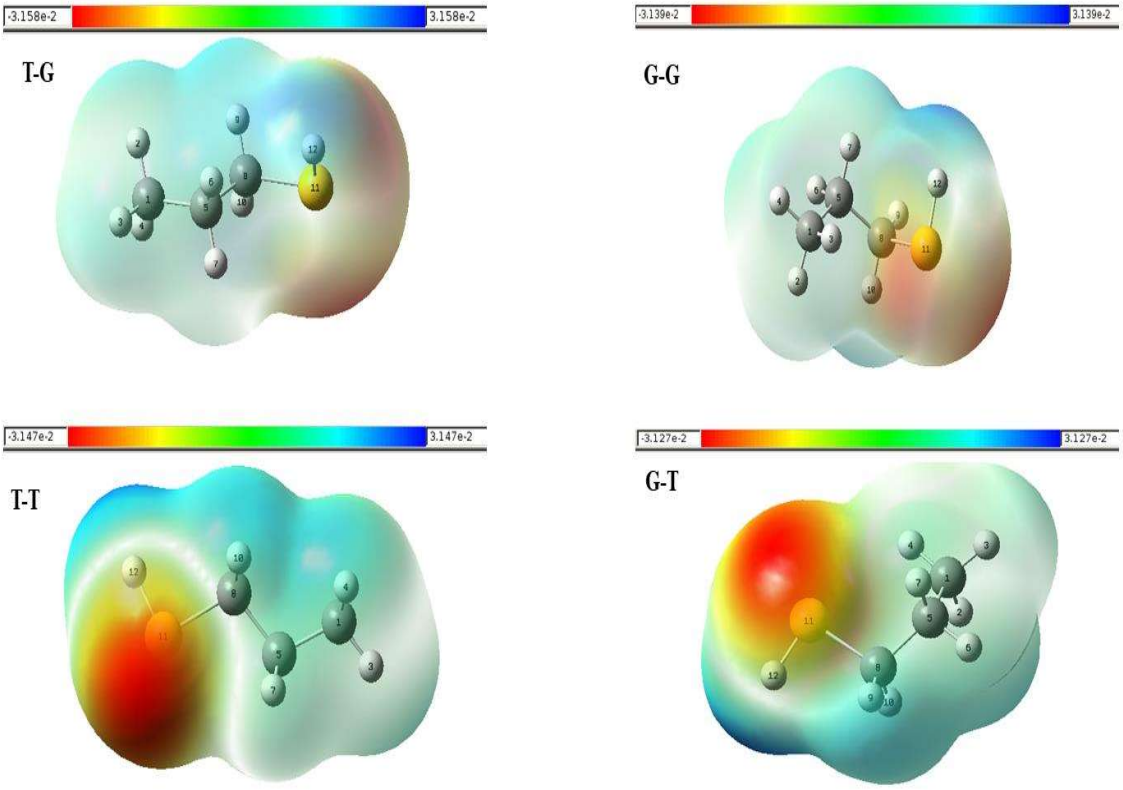

Figure 3.12 Electrostatic potential (ESP) surface plot of conformers of nP molecule at CCSD/cc-pVDZ level of theory.

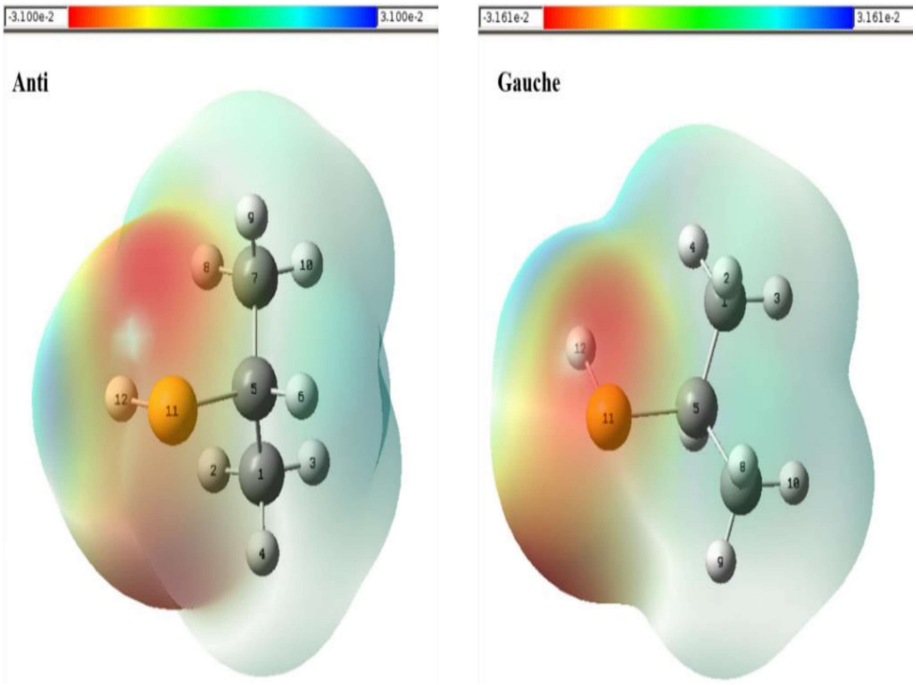

Figure 3.13 Electrostatic potential (ESP) surface plot of conformers of 2P at CCSD/cc-pVDZ level of theory.

Similar to the nP molecule, the 2P molecule showed a similar ESP map as shown in Fig. 3.13, and the charges corresponding to each atom of 2P are summarized in Table 3.8. In the case of the 2P molecule, the sulfur atom (S_{11}) is the most electrophilic center in the gauche conformer, whereas it is the least electrophilic in its anti-conformer. However, the carbon center (C_1) is the most electrophilic in anti-conformer, and it becomes the second most electrophilic center in gauche-conformer. Similar to nP, in 2P also, the C_5 atom is highly nucleophilic in both the conformers. Variation in nucleophilicity or electrophilicity center is mainly affected by the interaction of the electron-rich and electron-deficient centers of the molecules. NBO results validate these predictions very well, and the same are summarized below.

3.3.2 Mullikan charge (MC) analysis

MCA helps to analyze charge mobility and electronegativity processes within the molecule [128]. Mullikan charges (MC) were computed for the T–G, T–T, G–G, and G–T conformers of nP and for conformers of the 2P molecule, which are given in Table 8. Mullikan charges on the sulfur atom are negative for all conformers of the nP molecule. The values of the negative MC on the sulfur atom of T–G and G–T conformers are lower than in the T–T conformer, and hydrogen atoms 9 and 10 attain the maximum positive MC, indicating strong interactions that were well visualized in the NCI plot given in Fig. 3.7 and 3.11. In the case of the G–G conformer, the MC charge on the sulfur atom is positive and other atoms also have positive MC charges means atoms are weak in participation of interactions as compared to T–T and T–G conformer. NBO calculations also justified the delocalization of sulfur electrons into the antibonding molecular orbital of the C–$H_{9/10}$ bond, thereby making the T–G conformer more stable than the other two conformers of the nP molecule. These MCA calculations were further supported by the NBO calculations described below.

Table 3.8 Absolute values of electrostatic potential charge (ESP) and Mullikan charges (MC) on the atom of the conformers of nP and 2P molecules at CCSD/cc-pVDZ level of theory (All values are expressed in atomic units and parenthesis contains Mullikan charge)

Atom label[&]	nP				2P	
	T-T	G-G	T-G	G-T	Gauche	Anti
1 C of CH_3	-0.424 (-0.061)	-0.176 (0.059)	-0.223 (-0.062)	-0.203 (-0.066)	-0.371 (0.002)	-0.503 (0.004)
2 H of CH_3	0.108 (0.036)	0.055 (0.030)	0.047 (0.034)	0.042 (0.035)	0.093 (0.046)	0.146 (0.032)

3 H of CH_3	0.091 (0.040)	0.036 (0.054)	0.055 (0.041)	0.035 (0.037)	0.113 (0.036)	0.135 (0.037)
4 H of CH_3	0.108 (0.036)	0.036 (0.036)	0.032 (0.036)	0.081 (0.050)	0.098 (0.035)	0.114 (0.050)
5 C of CH_2-CH_3	0.259 (0.093)	0.134 (0.079)	0.272 (-0.073)	0.279 (-0.094)	0.216 (-0.281)	0.277 (-0.286)
6 H of CH_2-CH_3	0.021 (0.044)	-0.023 (0.035)	-0.048 (0.032)	-0.043 (0.037)	0.032 (0.063)	0.120 (0.068)
7 H of CH_2-CH_3	0.021 (0.044)	0.005 (0.031)	-0.057 (0.045)	-0.005 (0.042)	-0.275 (-0.018)	-0.503 (0.004)
8 C of CH_2-SH	-0.297 (-0.156)	-0.098 (0.150)	-0.089 (-0.162)	-0.284 (-0.143)	0.120 (0.047)	0.146 (0.032)
9 H of CH_2-SH	0.127 (0.060)	0.041 (0.070)	0.029 (0.068)	0.110 (0.061)	0.092 (0.052)	0.114 (0.050)
10 H of CH_2-SH	0.127 (0.060)	0.129 (0.072)	0.124 (0.072)	0.125 (0.059)	0.068 (0.042)	0.135 (0.037)
11 S	-0.345 (-0.075)	-0.329 (0.107)	-0.321 (-0.099)	-338 (-0.084)	-0.376 (-0.092)	-0.369 (-0.093)
12 H of S	0.204 (0.064)	0.188 (0.069)	0.178 (0.068)	0.200 (0.066)	0.190 (0.068)	0.189 (0.065)
& Note: Atom labels are as per the Fig. 2 and 3						

3.3.3 Natural bond orbital (NBO)

NBO calculations were carried out to know the extent of interaction (inter or intramolecular) between different orbitals (donor or acceptor orbital) of the nP and 2P and also understanding the charge transfer phenomenon in terms of the second-order perturbation energy, E(2) [130]. The greater the E(2) values translate to greater interactions between each

orbital and vice versa. In the NBO analysis, the chemical interpretation of hyper-conjugative interactions and transfer of electron density from the filled orbital or filled lone-pair electron occurs. NBO results for nP and 2P molecules are summarized in Tables 3.9 and 3.10. It was found that the conformers G–G, T–T, and T–G become stable compared to the conformer G–T because the G–T conformer has fewer interactions than the G–G, T–T, and T–G conformers. The interaction of sulfur's lone pair of electrons with orbitals $\sigma^*C_8–H_9$ and $\sigma^*C_8–H_{10}$ takes place along with donation in a $\sigma^*C_5–C_8$ orbital in G–G, T–T, and T–G conformers. The sulfur atom of T–T conformer shows strong interactions with $\sigma^*C_8–H_9$ and $\sigma^*C_8–H_{10}$ orbitals through both lone pairs, whereas T–G conformer only interacts with the $\sigma^*C_8–H_9$ orbital because the $\sigma^*C_8–H_{10}$ orbital is not in close proximity with no donation of the electrons to the antibonding molecular orbital of the $C_8–H_{10}$ bond. This means that the lone pair of the sulfur atom strongly interacts with hydrogen atoms 9 and 10 in the T–T conformer, whereas they interact only with the H_9 hydrogen atom of the T–G conformer. This indicates that the sulfur atom has a significantly lower electron density in T–T than the T–G conformer rendering it the most robust electrophilic center in the T–T conformer. Moreover, the G–G conformer shows a strong interaction between $\sigma^*C_5–HC_8$ orbital and sulfur lone pair of electrons that gives maximum stabilization energy compared to other conformers of nP molecule. Furthermore, the sulfur atom of the G–G conformer interacts only with $\sigma^*C_8–H_9$ orbital and not with $\sigma^*C_8–H_{10}$ orbital. Based on these predictions, it is inferred that the Gibbs free energy (thermodynamically) favored conformers are G–G and T–G (thermodynamically), and the T–T conformer is favored by electrostatic interactions (i.e., kinetically).

Table 3.9 Summary of NBO analysis of conformers of nP molecule at CCSD/cc-pVDZ level of theory

Orbital Interaction[#]	Second order perturbation energy [E(2)] (kcal/mol)			
	T-T	G-G	G-T	T-G
$\sigma_{1C-H2} \rightarrow \sigma^*_{5C-H7}$	4.32	4.57	4.46	4.32
$\sigma_{1C-H3} \rightarrow \sigma^*_{5C-H6}$	-	4.53	-	-
$\sigma_{1C-H3} \rightarrow \sigma^*_{5C-H8}$	4.89	-	5.20	4.88
$\sigma_{1C-H4} \rightarrow \sigma^*_{5C-H6}$	4.32	-	4.23	4.37
$\sigma_{1C-H4} \rightarrow \sigma^*_{5C-C8}$	-	5.19	-	-
$\sigma_{1C-H5} \rightarrow \sigma^*_{5C-C8}$	-	0.76	0.71	0.82
$\sigma_{1C-H5} \rightarrow \sigma^*_{5C-H6}$	-	-	2.39	-
$\sigma_{1C-H5} \rightarrow \sigma^*_{8C-H9}$	-	2.46	-	-
$\sigma_{1C-H5} \rightarrow \sigma^*_{8C-S11}$	3.74	-	-	4.30
$\sigma_{5C-H6} \rightarrow \sigma^*_{1C-H4}$	-	-	4.62	4.55
$\sigma_{5C-H6} \rightarrow \sigma^*_{1C-H3}$	-	4.56	-	-
$\sigma_{5C-H6} \rightarrow \sigma^*_{1C-H4}$	4.54	-	-	-
$\sigma_{5C-H6} \rightarrow \sigma^*_{8C-H10}$	4.58	-	-	4.68
$\sigma_{5C-H6} \rightarrow \sigma^*_{8C-S11}$	-	7.13	6.44	-
$\sigma_{5C-H7} \rightarrow \sigma^*_{1C-H2}$	4.54	4.48	4.49	4.54
$\sigma_{5C-H7} \rightarrow \sigma^*_{8C-H9}$	4.58	-	-	4.70
$\sigma_{5C-H7} \rightarrow \sigma^*8_{C-H10}$	-	4.62	4.54	-
$\sigma_{5C-C8} \rightarrow \sigma^*_{1C-H3}$	2.40	-	2.32	2.34
$\sigma_{5C-C8} \rightarrow \sigma^*_{1C-H4}$	-	2.34	-	-
$\sigma_{5C-C8} \rightarrow \sigma^*_{1C-C5}$	-	0.86	0.78	0.78
$\sigma_{5C-C8} \rightarrow \sigma^*_{8C-H9}$	-	0.51	0.57	-
$\sigma_{5C-C8} \rightarrow \sigma^*_{8C-H10}$	-	0.53	-	0.56
$\sigma_{5C-C8} \rightarrow \sigma^*_{11S-H12}$	-	-	0.70	-
$\sigma_{8C-H9} \rightarrow \sigma^*_{1C-C5}$	-	4.65	4.81	-
$\sigma_{8C-H9} \rightarrow \sigma^*_{5C-H7}$	4.36	-	4.34	4.21
$\sigma_{8C-H10} \rightarrow \sigma^*_{5C-H6}$	4.36	-	-	4.39
$\sigma_{8C-H10} \rightarrow \sigma^*_{5C-H7}$	-	4.36	4.34	-
$\sigma_{8C-H10} \rightarrow \sigma^*_{11S-H12}$	-	1.98	-	1.99
$\sigma_{8C-S11} \rightarrow \sigma^*_{5C-H6}$	-	3.00	3.46	-
$\sigma_{8C-S11} \rightarrow \sigma^*_{1C-C5}$	4.17	-	-	3.61
$\sigma_{8C-S11} \rightarrow \sigma^*_{11S-H12}$	0.59	0.67	0.56	0.65
$\sigma_{8C-H9} \rightarrow \sigma^*_{5C-H6}$	4.36	-	-	-
$\sigma_{8C-H10} \rightarrow \sigma^*_{5C-H6}$	4.36	-	-	-
$\sigma 11S-H12 \rightarrow \sigma^*_{5C-C8}$	2.75	-	2.96	-
$\sigma 11S-H12 \rightarrow \sigma^*_{8C-S11}$	1.01	1.15	0.92	1.19

σ11S-H12→σ*$_{8C-H10}$	-	2.90	-	2.96
LP(1)11S→σ*$_{5C-C8}$	-	1.29	-	1.26
LP(1)11S→σ*$_{1C-C5}$	0.51	-	-	-
LP(1) 11S→σ*$_{8C-H9}$	1.14	1.37	1.11	1.41
LP(1)11S→σ*$_{8C-H10}$	1.14	-	0.99	-
LP(2)11S→σ*$_{8C-H9}$	5.28	4.30	4.60	4.91
LP(2)11S→σ*$_{8C-H10}$	5.28	-	5.57	-
LP(2)11S→σ*$_{1C-C5}$	-	-	-	1.13
LP(2)11S→σ*$_{1C-H3}$	-	0.60	-	-
LP(2)11S→σ*$_{5C-C8}$	-	5.64	-	5.10
LP(2)11S→σ*$_{5C-H6}$	-	0.94	-	-
# Note: Atom labels are used as per the Fig. 2				

NBO analysis of the 2P molecule revealed 26 interactions in both the conformers (i.e., gauche and anti). The most intense interaction occurs between the lone pair of the sulfur atom and the antibonding molecular orbitals (ABMO) of the C–C and C–H bonds. In the anti-conformer, the lone pair of the sulfur atom strongly interacts with ABMOs of the C_1–C_5 and C_5–C_7 bonds, but in the gauche conformer, this happens with ABMOs of the C_1–C_5 and C_5–H_6 bonds. The sulfur atom of the 2P molecule has almost similar positive values to the ESPs, meaning both conformers have the same electrophilic center capacity. Overall, *E*(2) values for the anti-conformer are more prominent than the gauche conformer. Consequently, the anti-conformer becomes the most stable conformer out of all possible conformers of the 2P molecule, and the gauche conformer is the second most stable conformer. The NBO analysis agrees with the ESP, MCA, and FMO calculations for both nP and 2P molecules.

Table 3.10 Summary of NBO analysis of conformers of the 2P molecule at CCSD/cc-pVDZ level of theory (E(2) in kcal/mol and rest all in atomic unit)

Interacting orbitals[$]	Gauche			Anti		
	E(2)	$E_{(j)}$-$E_{(i)}$	F (i, j)	E(2)	$E_{(j)}$-$E_{(i)}$	F (i, j)
$\sigma_{C1-H2}\rightarrow\sigma^*_{C5-H6}$	4.48	1.39	0.071	4.52	1.38	0.071
$\sigma_{C1-H3}\rightarrow\sigma^*_{C5-S11}$	6.59	1.03	0.074	6.50	1.04	0.073
$\sigma_{C1-H4}\rightarrow\sigma^*_{C5-C7}$	4.78	1.30	0.070	4.79	1.30	0.071
$\sigma_{C1-C5}\rightarrow\sigma^*_{C5-H6}$	0.51	1.54	0.025	0.66	1.53	0.029
$\sigma_{C1-C5}\rightarrow\sigma^*_{C5-C7}$	1.15	1.45	0.037	0.99	1.45	0.034
$\sigma_{C1-C5}\rightarrow\sigma^*_{C7-H9}$	2.59	1.53	0.056	2.52	1.54	0.056
$\sigma_{C5-H6}\rightarrow\sigma^*_{C1-H2}$	4.39	1.38	0.070	4.49	1.37	0.070
$\sigma_{C5-H6}\rightarrow\sigma^*_{C7-H8}$	4.49	1.38	0.070	4.49	1.37	0.070
$\sigma_{C5-H6}\rightarrow\sigma^*_{S11-H12}$	-	-	-	2.10	1.12	0.043
$\sigma_{C5-C7}\rightarrow\sigma^*_{C1-H4}$	2.65	1.52	0.057	2.52	1.54	0.056
$\sigma_{C5-C7}\rightarrow\sigma^*_{C1-C5}$	1.06	1.45	0.035	0.99	1.45	0.034
$\sigma_{C5-C7}\rightarrow\sigma^*_{C5-H6}$	0.57	1.54	0.027	0.66	1.53	0.029
$\sigma_{C5-C7}\rightarrow\sigma^*_{S11-H12}$	0.87	1.27	0.030	-	-	-
$\sigma_{C5-S11}\rightarrow\sigma^*_{C1-H3}$	3.55	1.45	0.064	3.54	1.46	0.064
$\sigma_{C5-S11}\rightarrow\sigma^*_{C7-H10}$	4.02	1.46	0.068	3.54	1.46	0.064
$\sigma_{C5-S11}\rightarrow\sigma^*_{S11-H12}$	0.69	1.20	0.026	0.76	1.20	0.027
$\sigma_{C7-H8}\rightarrow\sigma^*_{C5-H6}$	4.38	1.39	0.070	4.52	1.38	0.071
$\sigma_{C7-H9}\rightarrow\sigma^*_{C1-C5}$	4.73	1.30	0.070	4.79	1.30	0.071
$\sigma_{C7-H10}\rightarrow\sigma^*_{C5-S11}$	5.77	1.04	0.069	6.50	1.04	0.073
$\sigma_{S11-H12}\rightarrow\sigma^*_{C5-C6}$	-	-	-	2.84	1.42	0.057
$\sigma_{S11-H12}\rightarrow\sigma^*_{C5-C7}$	2.77	1.33	0.054	-	-	-

$\sigma_{S11\text{-}H12} \rightarrow \sigma^*_{C5\text{-}S11}$	1.08	1.07	0.030	1.24	1.08	0.033
LP(1) $S11 \rightarrow \sigma^*_{C1\text{-}C5}$	1.16	1.42	0.036	1.47	1.42	0.041
LP(1) $S11 \rightarrow \sigma^*_{C1\text{-}C7}$	-	-	-	1.47	1.42	0.041
LP(1) $S11 \rightarrow \sigma^*_{C5\text{-}H6}$	1.23	1.51	0.039	-	-	-
LP(1) $S11 \rightarrow \sigma^*_{C7\text{-}H10}$	0.52	1.49	0.025	-	-	-
LP(2) $S11 \rightarrow \sigma^*_{C1\text{-}H3}$	1.25	1.05	0.033	1.30	1.05	0.033
LP(2) $S11 \rightarrow \sigma^*_{C1\text{-}C5}$	4.85	0.99	0.062	4.55	0.99	0.060
LP(2) $S11 \rightarrow \sigma^*_{C5\text{–}C7}$	-	-	-	4.55	0.99	0.060
LP(2) $S11 \rightarrow \sigma^*_{C5\text{-}H6}$	4.86	1.08	0.065	-	-	-
LP(2) $S11 \rightarrow \sigma^*_{C7\text{-}H10}$	-	-	-	1.30	1.05	0.033
$Note: atomic labels are used as per the Fig. 3.3						

3.3.4 Frontier molecular orbital (FMO)

The kinetic stability depends on the HOMO–LUMO (H–L) gap [130]. Values of H–L gaps define the chemical reactivity of a molecule. A lower value of the H–L gap indicates intense reactivity of the molecular system and vice versa. Energy parameters of the frontier molecular orbitals are summarized in Table 3.11 and graphically represented in Fig. 3.14. The H–L gap for T–T and G–T conformers is significantly smaller, indicating relatively higher reactivity than the T–G and G–G conformers of the nP molecule. Hence T–G and G–G are inferred as the most stable conformers followed by the T–T conformer and G–T is the least stable conformer of the nP molecule. For the nP molecule, our calculated dipole moment for the T–G conformer perfectly agrees with the experimental value 1.60 D [120], as shown in Table 3.11. Out of the four conformers, G–G has the maximum dipole moment (1.72 D), followed by the T–G conformer.

Table 3.11 Calculated energy parameters of conformers of nP and 2P molecules at CCSD/cc-pVDZ level of theory.

Energy Parameter ↓	nP				2P	
	T-G#	G-G	T-T	G-T	Anti#	Gauche
E_{HOMO} (in kcal/mol)	-220.46	-220.85	1226.62	1226.61	-220.23	-219.99
E_{LUMO} (in kcal/mol)	97.73	99.00	16.01	16.18	98.90	95.98
H-L gap (in kcal/mol)	318.19	319.85	-1210.61	-1210.43	317.43	315.96
Dipole moment (in D)	1.58 (1.60)	1.72	1.51	1.48	1.766 (1.61)	1.770
Hardness (η)	159.10	159.73	-605.31	-605.22	158.72	157.98
Chemical Potential (μ)	-61.37	-60.73	621.32	621.40	-60.67	-62.01
Electronegativity (χ)	61.37	60.73	-621.32	-621.40	60.67	62.01
Elecrophilicity Index (ω)	11.84	11.54	-318.88	-319.01	11.60	12.17
#Note: experimental values in parenthesis						

FMO calculation was also done for the 2P molecule and given in Table 3.11 and Fig. 3.15. The anti-conformer has a more significant H–L gap than the gauche (315.96 kcal/mol) conformer rendering it more stable than the gauche conformer. Theoretically calculated dipole moment for 2P molecule has a significantly closer value to the experimental value (1.61 D) [127], and the same is given in Table 3.11. These predictions have excellent agreement with the ESP, MCA, and NBO analysis.

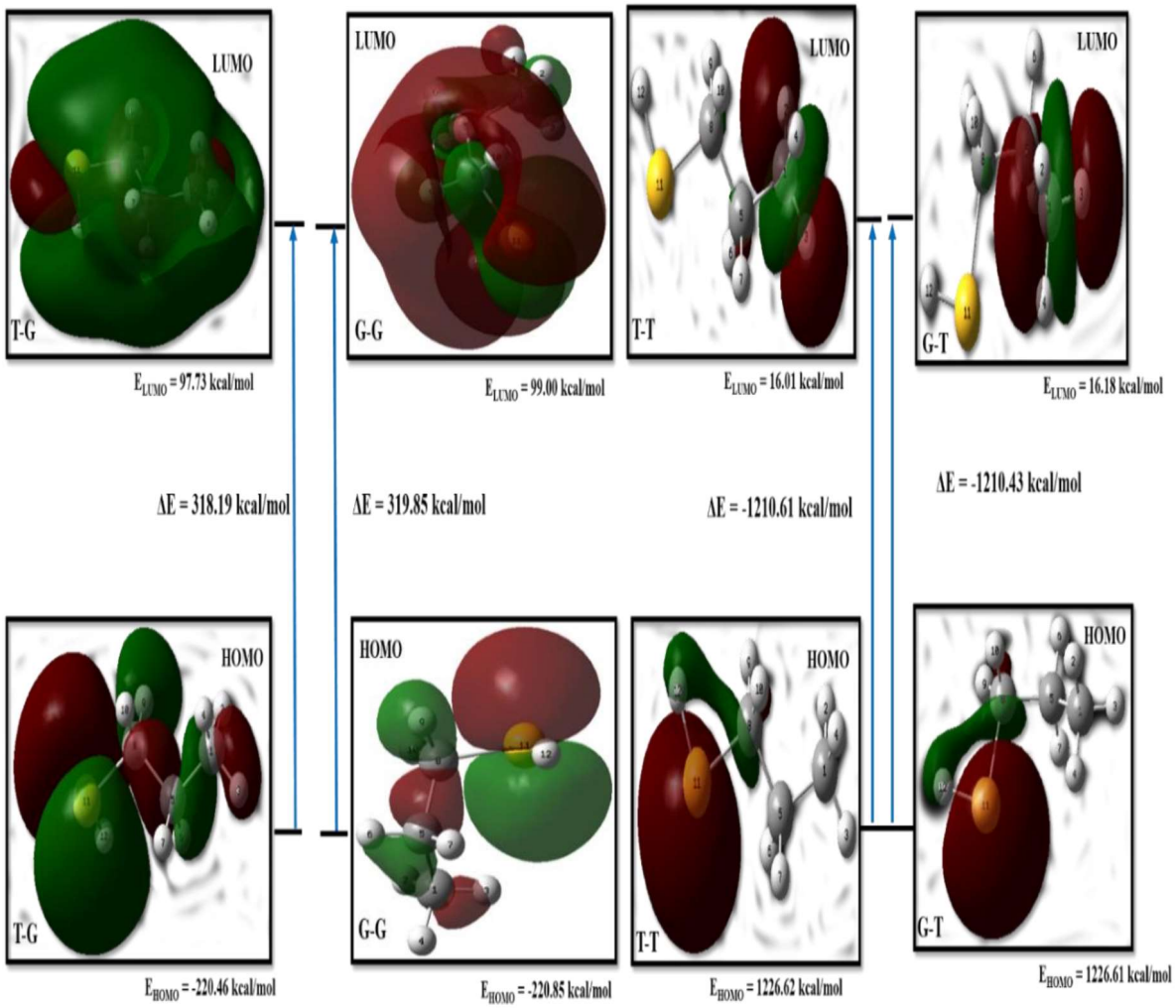

Figure 3.14 Schematic representation of frontier molecular orbitals of the different conformers of nP molecule at CCSD/cc-pVDZ level of theory.

3.3.5 Non-covalent interaction (NCI) plot

Non-covalent interaction plot gives a better way to visualize more precisely weaker interactions in molecules [132]. Herein the green color shows attractive non-covalent interaction between the donor and acceptor system. Conforms G-G and T-T shows more number of interactions as compared to T-G and G-T conformers, which gives clues about the

stability of the conformers as shown in Fig. 3.7 and 3.11. In the NCI plot of the T-T and G-G conformer, the sulfur atom interacts with C8 and C5 atoms and also the hydrogen atom of these carbon centers but this interaction is absent for the G-T conformer. Conformer T-G shows strong interactions with the hydrogen atom of the C_8 other than this no interaction was found. So the conformer with a higher number of interactions got the higher stability and they are referred to as kinetically favorable conformers.

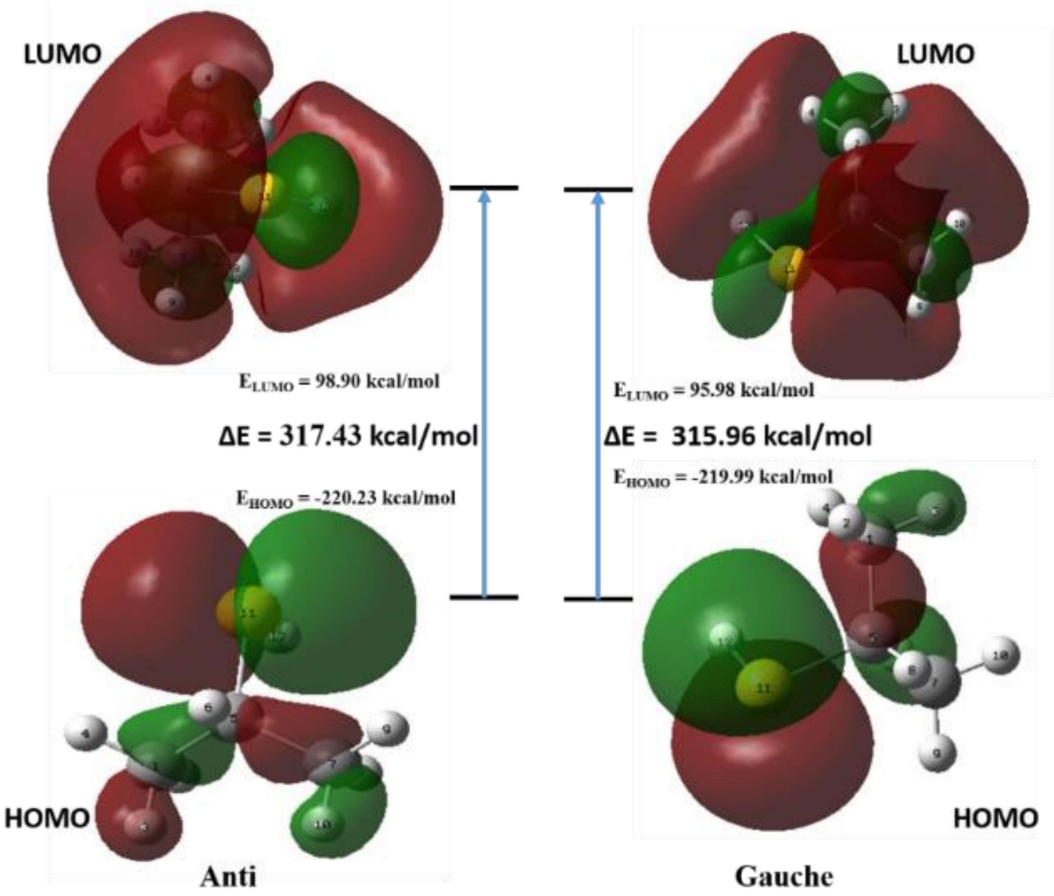

Figure 3.15 Schematic representation of frontier molecular orbitals of the different conformers of 2P molecule at CCSD/cc-pVDZ level of theory.

Thus, the conformer T-T is a kinetically favorable conformer, and the conformer T-G and G-G is the thermodynamically favorable conformer because it attains the lowest energy in possible conformers of the nP molecule. NCI plot of 2P conformers also shows weak interactions between lone pair and the two adjacent carbon atoms in both anti and gauche conformers of 2P molecule. Gauche conformer shows one additional weak interaction because of the active participation of the sulfur's lone pair and antibonding molecular orbital of the C_1-H_4 bond. A similar kind of interaction is also found in the anti-conformer of the 2P molecule with one additional interaction that was observed between the lone pair of electrons of sulfur and the ABMO of the C_7-H_9 bond. NCI plots of the weak interactions reinforced very well with results of the MCA, ESP, FMO, and NBO analysis.

3.4 Conclusion

The minimum energy conformer of nP and 2P was identified by rigorously exploring the conformational space pertaining to the dihedral angles. Adequate justification was given for the two conformers with the lowest energies. With the meticulous analysis and justification reported herein, the hitherto existing ambiguity in the computational literature is expected to cease. In summary,

• Four (T–G, G–G, T–T, and G–T) and two (anti and gauche) minimum energy conformers are found for nP and 2P molecules.

• Out of four conformers of the nP molecule, T–G is the global minimum with three local minima G–G, T–T, and G–T.

• In the conformational analysis of nP, the role of the C–C and C–S bonds was seen to be highly crucial in determining the energy of the conformer.

• Conformational analysis of nP molecule with T–T conformer as the starting geometry matched well with the experimental values vis-à-vis the G–G conformer as the starting geometry.

• Conformational stability of nP and 2P molecules was corroborated through NBO, FMO, MCA, ESPM, and NCI analysis.

• Our calculated geometrical parameters and rotational barriers for nP and 2P molecules excellently matched with the experimental results.